# Phase behavior of a family of continuous two-dimensional $n$-vector models with $n=2$, 3, and 4

E. Lomba, N. G. Almarza, and C. Martín
*Instituto de Química Física Rocasolano, CSIC, Serrano 119, E-28006 Madrid, Spain*
(Received 10 October 2007; published 6 December 2007)

In this work we investigate the phase behavior of a family of continuous bidimensional $n$-vector models (with $n=2$, 3, and 4) using Monte Carlo simulation. In all cases we detect the presence of a defect mediated order-disorder transition of the Berezinskii-Kosterlitz-Thouless type with critical temperatures that decrease with the spin dimensionality. Coupled with the order-disorder transition a gas-liquid equilibrium is found at low temperatures. Here one observes that the stability region of the liquid phase shrinks with the growing spin dimensionality, in parallel with a decrease in magnitude of the angular averaged spin-spin interaction.

DOI: 10.1103/PhysRevE.76.061107 PACS number(s): 64.60.Cn, 05.70.Fh

## I. INTRODUCTION

The presence of an unusual order-disorder transition in the two-dimensional $XY$ model has been known since the pioneering works of Berezinskii [1,2] and Kosterlitz and Thouless [3]. More generally, it has been found that similar transitions appear in lattice models of particular relevance in field theory and elementary-particle physics, such as the bidimensional $\mathbb{R}P^{n-1}$ (real projective space in $n$ dimensions), in which the lattice Hamiltonian can be written as [4,5]

$$H = -n\Sigma_{x,\mu}|\boldsymbol{\sigma}(x)\cdot\boldsymbol{\sigma}(x+e_\mu)|^2, \quad \mu = 1,2, \tag{1}$$

where $\boldsymbol{\sigma}(x)$ is a real $n$-component vector of unit length, and $e_\mu$ is a unit lattice vector in the direction $\mu$. When $n=2$ we are back to the $XY$ model and $n=3$ yields the Lebwohl-Lasher model [6], introduced in the liquid crystal literature to describe qualitatively the isotropic-nematic transition. This latter model, is nothing but a two-dimensional lattice version of the Maier-Saupe model [7,8]. The presence of a Berezinskii-Kosterlitz-Thouless (BKT) transition in the lattice models for $n=3$ and $n=40$ was investigated by Kunz and Zumbach [5] by means of extensive Monte Carlo calculations, and the results were compared with the analytic $n=\infty$ limit [4]. A comparative study of the critical behavior of lattice $\mathbb{R}P^2$ and $\mathbb{R}P^3$ models was carried out some time ago by Caracciolo *et al.* [9,10]. More recently, Fariñas-Sanchez *et al.* provided further evidence of the presence of a topological defect mediated transition in the $\mathbb{R}P^2$ model [11], in consonance with the nonconventional transition exhibited by the $XY$ system [3].

Concerning continuum models, the authors in collaboration with Lado [12] have recently presented a study on the phase behavior of a bidimensional Maier-Saupe fluid (or continuous $\mathbb{R}P^2$ model) which was found to exhibit a BKT transition along with a low temperature gas-liquid transition. The model studied in the presence of an external disorienting field, $W_0$ (i.e., a field that, when positive in magnitude, favors particle orientations lying in the system plane), is closely related to the $XY$ model in the limiting case of $W_0 \to \infty$. The aim of this paper is to complement both the work of [12] and the studies performed in lattice models, providing a comparative Monte Carlo study of the phase behavior of continuous two-dimensional $\mathbb{R}P^{n-1}$ models with $n=2$, 3, and 4. In this way, we intend to illustrate the influence of spin dimensionality on the phase equilibria of these systems.

The rest of the paper is organized as follows. The model is described in detail in Sec. II. In Sec. III we briefly summarize the simulation algorithms needed to perform our study and, finally, in Sec. IV we present our most significant results.

## II. MODEL

We will consider a fluid composed of particles lying in a two-dimensional plane which interact via a hard sphere potential of diameter $\sigma$ with embedded $n$-dimensional spins, i.e.,

$$u(r_{ij},\omega_i,\omega_j) = u_{\mathrm{HS}}(r_{ij}) + u_{\mathrm{ang}}(r_{ij},\omega_i,\omega_j), \tag{2}$$

where $u_{\mathrm{HS}}(r)$ is a hard sphere interaction, and the angular interaction is described by

$$u_{\mathrm{ang}}(r,\omega_i,\omega_j) = -Ku_0(r)\frac{1}{n-1}[(\hat{s}_i\cdot\hat{s}_j)^2 n - 1] \tag{3}$$

with $\hat{s}_i=(s_{i_1},s_{i_2},\ldots,s_{i_n})$ being an $n$-dimensional unit vector describing the orientation of the spin in particle $i$. In Eq. (3) the spin coupling is defined by

$$u_0(r) = \frac{e^{-\kappa(r-\sigma)}}{r/\sigma} - \frac{e^{-\kappa(R-\sigma)}}{R/\sigma} \quad \text{for} \quad \sigma < r < R, \tag{4}$$

$$u_0(r) = 0 \quad \text{for} \quad r > R. \tag{5}$$

The interaction is truncated at $R=4\sigma$ for computational convenience and we have set the screening $\kappa\sigma=1$. Throughout the paper we will use reduced densities, defined as $\rho^* \equiv \rho\sigma^2$ and temperatures, $T^* \equiv k_B T/K$, where $k_B$ is Boltzmann's constant and $T$ is the absolute temperature.

Note that the angular-dependent interaction, as defined in Eq. (3), leads to a net vanishing angular average, i.e.,

 

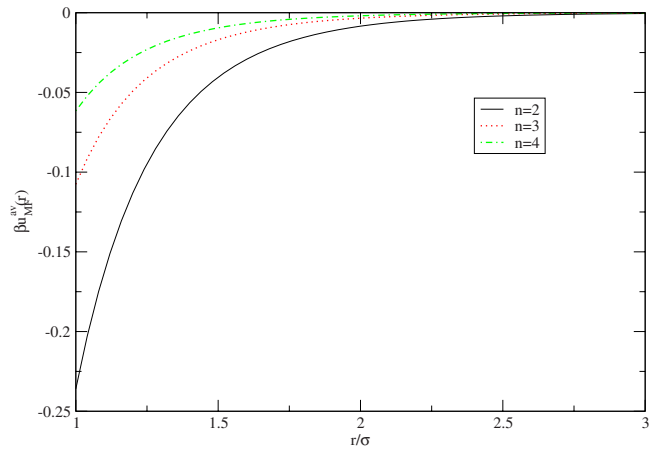


FIG. 1. (Color online) Angular average of the low density limit of the potential of mean force for coplanar $\mathbb{R}P^{n-1}$ spins.

$$\frac{1}{\Omega}\int_0^{\pi}\cdots\int_0^{2\pi} u_{\mathrm{ang}}(r,\omega_i,\omega_j) \times \sin^{n-2}\phi_1^i \sin^{n-3}\phi_2^i \cdots \sin\phi_{n-2}^i d\phi_1^i d\phi_2^i \cdots d\phi_{n-1}^i = 0, \tag{6}$$

where the solid angle differential element in hyperspherical coordinates is given by

$$d\omega_i = \sin^{n-2}\phi_1^i \sin^{n-3}\phi_2^i \cdots \sin\phi_{n-2}^i d\phi_1^i d\phi_2^i \cdots d\phi_{n-1}^i \tag{7}$$

and

$$\Omega = \frac{n\pi^{n/2}}{\Gamma(n/2+1)} \tag{8}$$

with $\Gamma$ being the gamma function. This is a general feature of many angular interaction potentials, such as those derived from the standard multipole expansion. However, in order to assess whether the spin-spin correlations will originate a net attraction or not, it is better to take a look at the angular average of the low density limit of the potential of mean force, namely

$$\beta u_{\mathrm{MF}}^{\mathrm{av}}(r) = -\ln\langle \exp[-\beta u_{\mathrm{ang}}(r,\omega_i,\omega_j)]\rangle_{\omega_i,\omega_j}, \tag{9}$$

where $\beta = 1/k_BT$, which we have plotted in Fig. 1 for $n=2$, 3, and 4 at $T^*=1$. It is readily seen from this figure that the magnitude of the effective attractive interaction potential shrinks as dimensionality increases. One should expect a visible fall in the gas-liquid critical temperature, until the equilibrium finally disappears as $n\to\infty$. Note, however, that if one plots $u_{\mathrm{MF}}^{\mathrm{av}}(r)/u_{\mathrm{MF}}^{\mathrm{av}}(\sigma)$ all curves are practically independent of $n$, i.e., the range of the averaged interaction is hardly dependent on spin dimensionality.

## III. SIMULATION ALGORITHMS

In a continuum model such as the one we are dealing with, Monte Carlo moves include both particle displacements and orientational moves. The former are carried out following the standard procedure, whereas for the latter we have implemented a local orientational update algorithm along the lines suggested in Refs. [13,12] together with a cluster algorithm [12] developed following the ideas of Swendsen and Wang [14]. In order to reduce the number of states to simulate and perform the finite size scaling analysis, we have resorted to the optimized histogram reweighting technique following the prescriptions of Ferrenberg and Swendsen [15] and Holm and Janke [16]. A detailed description of the algorithm can be found in [13]. As to the orientational moves, in what follows we summarized the main steps of the two algorithms involved, written explicitly for $n$-dimensional spins.

### A. Cluster algorithms

The steps to define clusters in our simulation sample and then perform cluster moves are essentially those outlined in Ref. [13], except for the fact that we will be dealing with $n$ dimensions. The algorithm to define a cluster can be sketched as follows:

(1) Choose a unit $n$-dimensional vector $\hat{R}$ to denote a hyperplane with respect to which we will perform reflections of the spin vectors.

(2) For a given particle $i$, decompose its spin vector $\hat{s}_i$ such that

$$\hat{s}_i = \hat{s}_{i_\parallel} + \hat{s}_{i_\perp}$$

with $\hat{s}_{i_\parallel} = (\hat{s}_i\cdot\hat{R})\hat{R}$.

(3) The new vector resulting from the reflection operation has the component parallel to $\hat{R}$ with opposite sign and an identical perpendicular component, i.e.,

$$\hat{s}_i^{(n)} = \hat{s}_{i_\perp} - (\hat{s}_i\cdot\hat{R})\hat{R},$$

$$\hat{s}_i^{(n)} = \hat{s}_i - 2(\hat{s}_i\cdot\hat{R})\hat{R}. \tag{10}$$

As a consequence, a reflection of two spin orientations does not affect the corresponding spin-spin interaction energy, since

$$\hat{s}_i^{(n)}\cdot\hat{s}_j^{(n)} = \hat{s}_i\cdot\hat{s}_j.$$

On the other hand, the change in energy when modifying the orientation of a single particle is given by

$$\beta u_{ij} - \beta u_{ij,n} = \frac{-4n\beta K u_0(r)}{n-1}(\hat{s}_i\cdot\hat{R})(\hat{s}_j\cdot\hat{R}) \times[(\hat{s}_i\cdot\hat{s}_j) - (\hat{s}_i\cdot\hat{R})(\hat{s}_j\cdot\hat{R})]. \tag{11}$$

(4) With this in mind, one defines the quantity

$$\phi_{ij} = 1 - \min\left[1, \exp\left(\frac{-4n\beta K u_0(r)}{n-1}(\hat{s}_i\cdot\hat{R})(\hat{s}_j\cdot\hat{R}) \times[(\hat{s}_i\cdot\hat{s}_j) - (\hat{s}_i\cdot\hat{R})(\hat{s}_j\cdot\hat{R})]\right)\right], \tag{12}$$

so that two particles $i$ and $j$ will be linked if

$$\zeta > \phi_{ij}, \tag{13}$$

where $\zeta$ is a uniform random number such that $0 \leq \zeta \leq 1$.

Once all the clusters have been constructed running the previous algorithm over all particle pairs, one should perform a reflection of all the spins in every cluster with a probability 1/2.

### B. Local update algorithm

In this case the algorithm closely follows the scheme outlined in [12].

(1) Randomly choose a particle $j$ whose orientation is described by a unit vector $\hat{\mathbf{s}}_j$ of components $s_j^\alpha$ $(\alpha = 1, \ldots, n)$.

(2) Determine the orientation $\hat{\mathbf{s}}_j^{\min}$ for which the interaction of the chosen particle with the remaining ones corresponds to a minimum. This step is easily carried out in our case if one notices that the relevant energy

$$\beta u_j = -\frac{n}{n-1}\beta K \sum_i u_0(r_{ij})(\hat{\mathbf{s}}_i \cdot \hat{\mathbf{s}}_j)^2 \tag{14}$$

[where the additive $1/(n-1)$ term has been dropped since it does not affect the orientational move] can be recast in matrix form as

$$\beta u_j = \hat{\mathbf{s}}_j \cdot \mathbf{A}^{(j)} \cdot \hat{\mathbf{s}}_j, \tag{15}$$

where

$$A_{\gamma\upsilon}(j) = -\frac{n}{n-1}\beta K \sum_i u_0(r_{ij}) s_i^\gamma s_i^\upsilon \tag{16}$$

with $\gamma, \upsilon = 1, \ldots, n$. By diagonalization we have

$$\beta u_j = \sum_\gamma \lambda_\gamma (s_j'^{\gamma})^2, \tag{17}$$

where the $\lambda_\gamma$ are the eigenvalues of $\mathbf{A}^{(j)}$ and $\hat{\mathbf{s}}_j' = \mathbf{U} \cdot \hat{\mathbf{s}}_j$, with $\mathbf{U}$ being the matrix formed by the eigenvectors of $\mathbf{A}^{(j)}$. Thus, minimizing (17) with the constraint that $\hat{\mathbf{s}}_j$ be normalized, one finds that the minimum energy corresponds to the minimum eigenvalue of $\mathbf{A}^{(j)}$, $\lambda_{\min}$.

(3) With the energy minimum thus calculated, pick a random orientation described by a vector $\hat{\mathbf{s}}_j$ and evaluate the ratio

$$\xi = \frac{\exp(-\beta u_j)}{\exp(-\beta u_j^{\min})} = \exp[-(\beta u_j - \lambda_{\min})]. \tag{18}$$

(4) Finally, generate a uniformly distributed random number $\zeta$, $0 \leq \zeta \leq 1$, and accept the new orientation if $\zeta \leq \xi$; otherwise, return to the previous step.

### C. Orientational order

In order to monitor the orientational order of the sample we need the $n$-dimensional generalization of Saupe's tensor [17], which reads as

$$T_{\alpha\beta} = \frac{1}{n-1}\left(\frac{1}{N}\sum_{i=1}^{N}(n s_i^\alpha s_i^\beta - \delta_{\alpha\beta})\right), \quad \alpha, \beta = 1, \ldots, n, \tag{19}$$

where $s_i^\alpha$ are the components of a unit $n$-dimensional vector denoting the orientation of the particle $i$, $N$ is the number of particles, and $\delta_{\alpha\beta}$ is Kronecker's delta. Note that this tensor is traceless, i.e.,

$$\mathrm{Tr}\{\mathbf{T}\} = 0$$

by which

$$\sum_{i=1}^{n} \lambda_i = 0$$

is also fulfilled by the eigenvectors of $\mathbf{T}$, $\lambda_i$. The order-disorder transition will be monitored by means of the largest eigenvalue of $\mathbf{T}$, which will be our order parameter $\lambda_+ = S$. The corresponding susceptibility

$$\chi = N(\langle \lambda_+^2 \rangle - \langle \lambda_+ \rangle^2) \tag{20}$$

will be a key quantity to signal the presence of a BKT order-disorder transition.

### D. Liquid-vapor transition

For the purpose of calculating the liquid-vapor equilibrium we have followed the same technique used in Ref. [12] which is based on Wang and Landau's method [18,19]. In each simulation run the volume and the temperature are fixed, and a wide range of densities, number of particles, is sampled by introducing an appropriate preweighting factor (different from that used in grand canonical Monte Carlo simulations). In order to attain a nearly uniform sampling over the chosen density range, the preweighting factor is computed by a Wang-Landau-type method before running the actual sampling part of the simulation. Standard procedures [20,21] were used to perform the different kind of moves: insertion, deletion, translation, and orientational attempts. The acceptance criteria for moves implying changes in the number of particles followed the scheme given in [12].

Using this procedure we can compute the excess Helmholtz energy function of the system as a function of $N$, and subsequently derive the thermodynamics of the system. In order to extract the liquid-vapor equilibrium (LVE) we compute the value of the chemical potential, $\mu_0(T,L)$ that maximizes the fluctuations of the density for the chosen conditions of $L$ and $T$, $L$ being the length of the simulation box side. If LVE occurs, we expect that the probability distribution of the density at $\mu_0$, $\Pi(\rho|\mu_0, L, T)$, will exhibit two well-separated narrow peaks (each one corresponding to a different phase). If only one peak appears no LVE will be found at that temperature. The analysis can be performed employing the momenta of $\Pi(\rho|\mu_0, L, T)$, $m_i$, defined as

$$m_1 = \rho_m = \langle \rho \rangle = \frac{\int d\rho \Pi(\rho|\mu_0, L, T)\rho}{\int d\rho \Pi(\rho|\mu_0, L, T)}, \tag{21}$$

$$m_j = \langle (\rho - \rho_m)^j \rangle \quad \text{for} \quad j \geq 2. \tag{22}$$

Using these momenta we can compute

$$\delta\rho(T,L) = \sqrt{m_2} \tag{23}$$

and the parameter $G$, given by

$$G = \frac{1}{2}\left(3 - \frac{m_4}{m_2^2}\right). \tag{24}$$

In the thermodynamic limit $(L \to \infty)$ we expect to have the following behavior of $\delta\rho(T)$ and $G(T)$:

$$\lim_{L\to\infty} \delta\rho(T,L) = \begin{cases} \dfrac{\rho_l(T) - \rho_v(T)}{2} > 0, & T < T_c, \\ 0, & T \geq T_c, \end{cases} \tag{25}$$

$$\lim_{L\to\infty} G(T,L) = \begin{cases} 1, & T < T_c, \\ G_c, & T = T_c, \\ 0, & T > T_c, \end{cases} \tag{26}$$

where $\rho_l$ and $\rho_v$ represent the densities of the vapor and liquid phases, respectively; $G_c$ is a singular nontrivial value, which depends on the *universality class* to which the system pertains [22]. For the systems considered herein, the values $G^c$ are not known. The slope of $G(T,L)$ with $T$ when crossing the critical temperature increases with the system size. In order to estimate $T_c$ we followed the same strategy reported in [12], i.e., we define apparent critical temperatures, $T_c(L)$, as

$$G[T_c(L),L] = G_c^I, \tag{27}$$

where $G_c^I$ is the universal ratio for the Ising model in two dimensions, which is estimated to be [23] $G_c^I \approx 0.9160$.

In order to compute $T_c(L)$ from (27) we have made use of the simplified reweighting techniques reported in [12]. The extrapolation to estimate $T_c$ was performed following finite size scaling (FSS) methods [24] and will be commented on in the next section.

For temperatures below $T_c$ the densities of the vapor and liquid phases were computed fitting the results of $\rho_m(L,T)$ and $\delta\rho(L,T)$ to polynomials of $(1/L^2)$, e.g.,

$$\rho_m(T,L) = \rho_m(T) + \sum_i a_{\rho,i}(1/L^2)^i, \tag{28}$$

$$\delta\rho(T,L) = \delta\rho(T) + \sum_i a_{\delta\rho,i}(1/L^2)^i. \tag{29}$$

The densities of the coexisting phases are then taken as $\rho_i(T) = \rho_m(T) \pm \delta\rho(T)$.

## IV. RESULTS

In order to describe the order-disorder transition we have performed calculations for $n=2$ and 4 (results for $n=3$ have been taken from Ref. [12]) using samples of 400, 900, 1600, 2500, and 3600 particles for densities $\rho\sigma^2 = 0.5$, 0.6, 0.7, and 0.8 when $n=2$ and $\rho\sigma^2 = 0.7$ and 0.8 (0.6 lies too close to the liquid-vapor transition) when $n=4$. The evolution of the reduced excess constant volume specific heat per particle

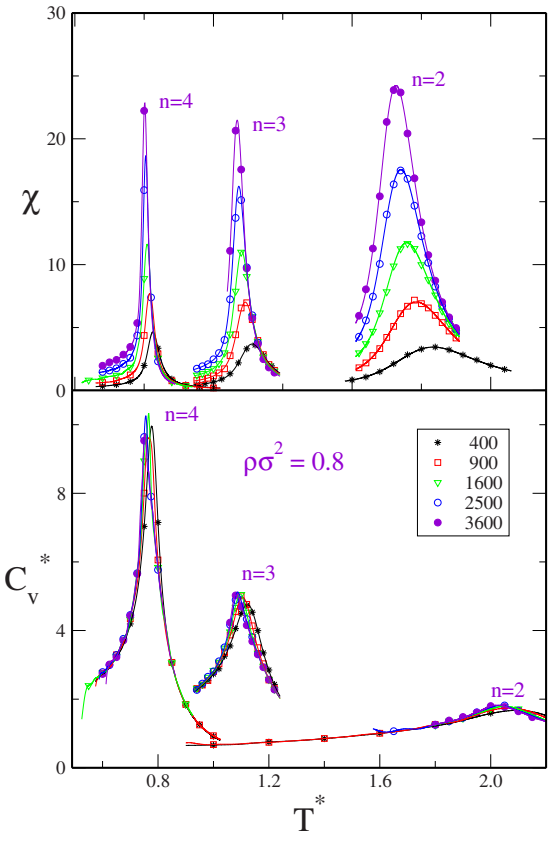


FIG. 2. (Color online) Reduced excess constant volume specific heat per particle in units of $k_B$ [Eq. (30)] and susceptibility [Eq. (20)] for the coplanar $\mathbb{R}P^{n-1}$ spin fluid for $n=2$, 3, and 4 and $\rho\sigma^2 = 0.8$. Symbols correspond to simulated states and the curves result from the histogram reweighting technique.

$$C_v^* = \frac{1}{NT^{*2}}[\langle (U/K)^2 \rangle - \langle (U/K) \rangle^2], \tag{30}$$

where $U$ is the excess internal energy, plotted in Fig. 2 together with the susceptibility calculated from the nematic order parameter—Eq. (20)—as an illustration of their behavior just for one representative density, $\rho\sigma^2 = 0.8$. Similar curves are obtained for other densities and are not included for brevity.

From a simple inspection of Fig. 2 one sees that the transition temperatures (as estimated from the maxima of $\chi$) substantially decrease with the spin dimension. As found in Ref. [12] for the $\mathbb{R}P^2$ model, one observes in all cases that the heat capacities reach a maximum near the transition temperature, but do not diverge. As mentioned by Kunz and Zumbach [5], one should expect the maximum to evolve into a cusp at the thermodynamic limit. This lack of divergence of $C_v^*$ when approaching criticality is in contrast with the behavior of the heat capacity at second-order phase transitions in two dimensions, which is known to exhibit a logarithmic divergence. Concerning the susceptibility, the considerable increase in this quantity with the sample size points to the

TABLE I. Transition temperatures and critical exponents $\eta$ and $\gamma/\nu$ for the planar $\mathbb{R}P^{n-1}$ spin fluid.

| $n$ | 2 | | | 3 | | | 4 | | |
|---|---|---|---|---|---|---|---|---|---|
| $\rho\sigma^2$ | $T_{\mathrm{BKT}}$ | $\eta$ | $\gamma/\nu$ | $T_{\mathrm{BKT}}$ | $\eta$ | $\gamma/\nu$ | $T_{\mathrm{BKT}}$ | $\eta$ | $\gamma/\nu$ |
| 0.50 | 0.82(10) | 0.35(3) | 1.84(4) | | | | | | |
| 0.60 | 1.06(4) | 0.30(1) | 1.81(4) | 0.51(3) | 0.29(3) | 1.70(9) | | | |
| 0.70 | 1.44(2) | 0.32(1) | 1.78(1) | 0.78(1) | 0.36(2) | 1.64(6) | 0.55(7) | 0.41(3) | 1.49(6) |
| 0.80 | 1.77(1) | 0.32(1) | 1.74(2) | 0.99(1) | 0.38(2) | 1.61(4) | 0.73(10) | 0.37(5) | 1.5(3) |

presence of a divergence and, consequently, an order-disorder transition should be expected. In fact, the value of the susceptibility at the maximum scales with the sample size as $\chi \propto L^{\gamma/\nu}$ as expected, and the values of the critical exponent ratio $\gamma/\nu$ thus computed are collected in Table I. These do not deviate much from the two-dimensional Ising model $\gamma/\nu=7/4$. Apparently, the estimated $\gamma/\nu$ values seem to decrease with rising dimensionality but the large statistical uncertainties for spin dimensions 3 and 4 do now allow to draw definite conclusions in this regard. On the other hand, the density dependence is also very small and remains somewhat masked by the statistical errors. Finally, it is worth mentioning that the susceptibility diverges for all temperatures below the transition temperature (as can be inferred from its sample size dependence) in agreement with the expected behavior in a BKT transition [5]. This, together with the lack of divergence of $C_v^*$, is the signature of the BKT transition.

If we now look at the cumulant constructed from the orientational order parameter, following Weber, Paul, and Binder [25]

$$g_4 = \langle \lambda_+^4 \rangle / \langle \lambda_+^2 \rangle^2,$$

$$g_2 = \langle \lambda_+^2 \rangle / \langle \lambda_+ \rangle^2, \tag{31}$$

we see again in Fig. 3 the same trends as in Fig. 2.

Employing once more the recipe of Ref. [12], we can perform a FSS analysis with the location of the maxima of the susceptibility, $T_m^*$, and the crossover temperatures of the cumulant, $T_\times^*$ (checking for the crossing of curves for sample sizes larger than 500 with the curve that corresponds to the 500 particle sample). To that purpose, the series of $T_m^*$ and $T_\times^*$ is fitted to a functional form [26]

$$T_{\mathrm{BKT}}^*(l) = T_{\mathrm{BKT}}^* + \frac{a}{(c + \ln l)^2}, \tag{32}$$

where $l=\sqrt{N}$ and $T_{\mathrm{BKT}}^*(l)$ is either $T_m^*(L)$ or $T_\times^*$. Additionally, following Tomita and Okabe [26], the value of the order parameter squared at the temperatures corresponding to the susceptibility maxima should scale as

$$\langle \lambda_+^2(l) \rangle = \frac{A l^{-\eta}}{(c + \ln l)^{2r}}. \tag{33}$$

Again, as in Ref. [12], we can drop the logarithmic corrections and take $\langle \lambda_+^2(l) \rangle \propto l^{-\eta}$. The results of these scaling fits are summarized in Table I. One sees immediately that the decrease of the critical temperature when going from $n=2$ to $n=3$ is associated with a corresponding moderate increase of the critical exponent $\eta$. The value of this latter exponent remains stable when going from $n=3$ to $n=4$, but the critical temperature further decreases. Note that Kunz and Zumbach obtained $\eta=0.4$ for the lattice version of the $\mathbb{R}P^2$ model [5] and Tomita and Okabe give $\eta=0.24$ for the $XY$ (i.e., $\mathbb{R}P^1$) model [26]. In our case we obtain $\eta \approx 0.3$ for the $\mathbb{R}P^1$ and $\eta \approx 0.4$ in the $\mathbb{R}P^2$ and $\mathbb{R}P^3$ cases. Our calculations are not accurate enough to discriminate better between the $n=3$ and $n=4$ cases. As for the density dependence of $\eta$, it is only statistically significant for the three-dimensional case at $\rho\sigma^2=0.6$. However, this point happens to be too close to the gas-liquid critical point for its critical estimates to be so reliable. Concerning the critical temperatures, in Fig. 4 we have plotted the transition temperatures appropriately scaled with dimensionality, namely, $nT_{\mathrm{BKT}}^*$. Interestingly, one observes that already the results for $n=3$ and $n=4$ scale rather well as $1/n$ in agreement with the findings for large $n$ values in lattice models [4,5].

Now, in order to describe the liquid-vapor equilibrium we have run an extensive series of simulations, essentially in the same conditions used in Ref. [12] with $n=2$ and $n=4$. As in the case of the order-disorder transition, data for $n=3$ have been directly taken from Ref. [12]. Different system sizes were used to extrapolate the thermodynamic limit values of

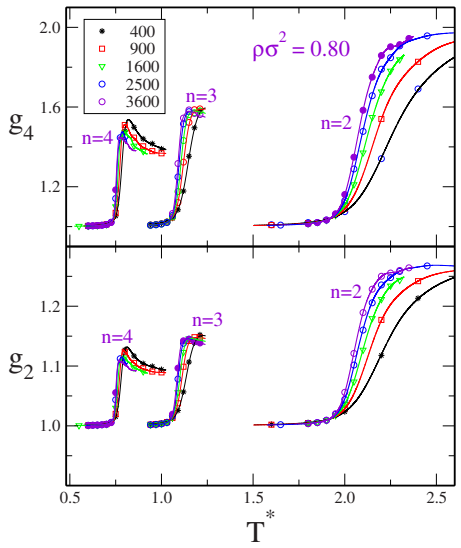


FIG. 3. (Color online) Size and temperature dependence of Binder's cumulants as defined in Eq. (31) for the coplanar $\mathbb{R}P^{n-1}$ spin fluid for $n=2$, 3, and 4 at $\rho\sigma^2=0.8$. Symbols correspond to simulated states and the curves result from the histogram reweighting technique.

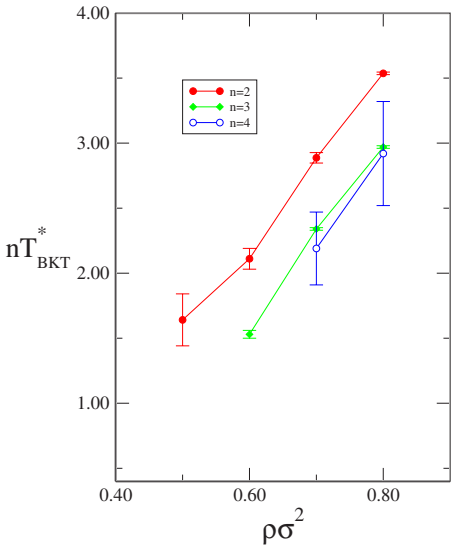


FIG. 4. (Color online) Transition temperatures scaled with dimensionality for the coplanar $\mathbb{R}P^{n-1}$ spin fluid for $n=2$, 3, and 4 at $\rho\sigma^2=0.8$. Lines are drawn as guides to the eyes.

the coexistence densities of the liquid vapor equilibria. In the vicinity of the critical points we used system sizes up to $L/\sigma=44$ to attain reliable estimates of $T_c$.

Estimates of LVE critical properties are summarized in Table II. We have fitted the apparent critical temperatures $T_c^*(L)$ to the following scaling law:

$$T_c^*(L) = T_c^* + a_t\left(\frac{1}{L}\right)^{b_t}. \tag{34}$$

Once $T_c^*$ is estimated, we use results for different sizes at $T_c^*$ to extrapolate $\rho_c^*$. The values of $\delta\rho(T_c,L)$ can be fitted to a scaling law of the type

$$\ln[\delta\rho(T_c^*,L)\sigma^2] = a_\delta - b_\delta \ln L, \tag{35}$$

where the ratio of critical exponents $\beta/\nu$ can be estimated from $b_\delta \approx \beta/\nu$. In the two-dimensional Ising universality class $\beta/\nu=0.125$, which deviates from the results in Table II. The value for $n=2$ agrees with the results for the $\mathbb{R}P^2$ model in the presence of an infinite disorienting field (i.e., coplanar spins) as it should be. As a general trend one observes that the $\beta/\nu$ tends to increase somewhat with the dimensionality. Also, from Table II it is apparent the decrease in the critical temperature (and a corresponding rise in $\rho_c$) with increasing spin dimensionality. The fall in $T_c^*$ is clearly in consonance with the decrease in the magnitude of the net attractive interaction with growing dimensionality (cf. Fig. 1).

Figure 5 illustrates the global changes in the phase equilibria we have already discussed. The LVE curves appear at lower $T^*$ and are shifted toward higher densities as the spin dimension is increased. One should expect the LV equilibrium to disappear as the spin dimensionality grows. Concerning the order-disorder transition, we also observe that the transition temperatures fall as the spin dimension rises. If the analysis of Kunz and Zumbach is correct [4,5], for $n=\infty$ one should expect, however, a very small but nonzero critical temperature. This is in contrast with the behavior of the two-dimensional classical $n$-vector model in the limit $n\to\infty$ (or equivalently the spherical model [27]) which is known not to exhibit any order-disorder transition [28]. Obviously, our limited calculations cannot shed new light on this issue.

TABLE II. Estimates of critical properties and liquid-vapor equilibrium for the planar $\mathbb{R}P^{n-1}$ spin fluid.

| $n$ | $T_c^*$ | $\rho_c^*$ | $b_t$ | $b_\delta$ |
|---|---|---|---|---|
| 2 | 0.594(3) | 0.427(1) | 1.2(2) | 0.22(3) |
| 3 | 0.542(3) | 0.524(10) | 1.04(10) | 0.28(4) |
| 4 | 0.504(8) | 0.62(2) | 1.0(2) | 0.32(7) |

In summary, we have presented the results of extensive Monte Carlo calculations to elucidate the influence of spin dimensionality on the phase behavior of the $\mathbb{R}P^{n-1}$ spin fluid for $n=2$, 3, and 4. From our study, it can be concluded that in all cases one finds a BKT transition for which $T_{\mathrm{BKT}}^*$ decreases with increasing dimensionality, apparently in accordance with a $1/n$ scaling. An additional LV equilibrium is found at low temperatures (as compared with $T_{\mathrm{BKT}}^*$) with a critical temperature whose value also diminishes as the spin dimensionality rises. This fall in the critical temperature is accompanied by a shift of the critical density to higher values. The fact that for higher spin dimensions one should lower the temperature to encounter the liquid phase is an immediate consequence of the shrinking magnitude of the average net attraction between $n$-dimensional spins when $n$ grows.

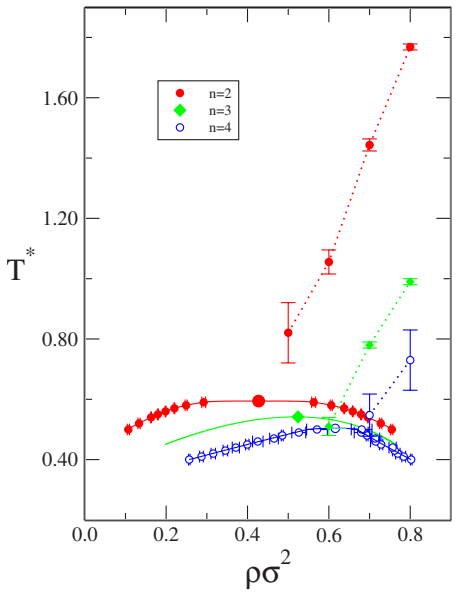


FIG. 5. (Color online) Simulation results for the phase diagram of the planar $\mathbb{R}P^{n-1}$ spin fluid for $n=2$, 3, and 4. Symbols joined with dotted lines correspond to the states at which the BKT transition takes place and the line separates orientationally disordered states (lower densities) from states with quasi-long-range order (higher density, quasinematic states).

**ACKNOWLEDGMENTS**

The authors gratefully acknowledge financial support from the Dirección General de Investigación Científica y Técnica under Grant No. FIS2004-02954-C03-01 and the Dirección General de Universidades e Investigación de la Comunidad de Madrid under Grant No. S0505/ESP/0299, program MOSSNOHO-CM.

[1] V. Berezinskii, Sov. Phys. JETP **34**, 610 (1972).
[2] V. Berezinskii, Sov. Phys. JETP **32**, 493 (1971).
[3] J. M. Kosterlitz and D. J. Thouless, J. Phys. C **5**, L124 (1972).
[4] H. Kunz and G. Zumbach, J. Phys. A **22**, L1043 (1989).
[5] H. Kunz and G. Zumbach, Phys. Rev. B **46**, 662 (1992).
[6] P. A. Lebwohl and G. Lasher, Phys. Rev. A **6**, 426 (1972).
[7] W. Maier and A. Saupe, Z. Naturforsch. A **14A**, 882 (1959).
[8] W. Maier and A. Saupe, Z. Naturforsch. A **15A**, 287 (1960).
[9] S. Caracciolo, R. G. Edwards, A. Pelissetto, and A. D. Sokal, Nucl. Phys. B (Proc. Suppl.) **30A**, 815 (1993).
[10] S. Caracciolo, R. G. Edwards, A. Pelissetto, and A. D. Sokal, Phys. Rev. Lett. **71**, 3906 (1993).
[11] A. I. Fariñas-Sanchez, R. Paredes, and B. Berche, Phys. Lett. A **308**, 461 (2003).
[12] E. Lomba, C. Martín, N. G. Almarza, and F. Lado, Phys. Rev. E **71**, 046132 (2005).
[13] E. Lomba, C. Martín, and N. Almarza, Mol. Phys. **101**, 1667 (2003).
[14] R. H. Swendsen and J.-S. Wang, Phys. Rev. Lett. **58**, 86 (1987).
[15] A. M. Ferrenberg and R. H. Swendsen, Phys. Rev. Lett. **63**, 1195 (1989).
[16] C. Holm and W. Janke, Phys. Rev. B **48**, 936 (1993).
[17] A. Saupe, Z. Naturforsch. A **19A**, 161 (1964).
[18] F. Wang and D. P. Landau, Phys. Rev. Lett. **86**, 2050 (2001).
[19] F. Wang and D. P. Landau, Phys. Rev. E **64**, 056101 (2001).
[20] M. Allen and D. Tildesley, *Computer Simulation of Liquids* (Clarendon, Oxford, 1987).
[21] D. Frenkel and B. Smit, *Understanding Molecular Simulation* (Academic, London, 2002).
[22] K. Binder, Z. Phys. B **43**, 119 (1981).
[23] G. Kamieniarz and H. Blote, J. Phys. A **26**, 201 (1993).
[24] N. B. Wilding, Phys. Rev. E **52**, 602 (1995).
[25] H. Weber, W. Paul, and K. Binder, Phys. Rev. E **59**, 2168 (1999).
[26] Y. Tomita and Y. Okabe, Phys. Rev. B **65**, 184405 (2002).
[27] H. Stanley, Phys. Rev. **179**, 570 (1969).
[28] T. H. Berlin and M. Kac, Phys. Rev. **86**, 821 (1952).